A new biomimetic assay reveals the temporal role of matrix stiffening in cancer cell invasion

(15,900 characters – no spaces)

Ralitza Staneva[1,2*], Federica Burla[3*], Gijsje H. Koenderink[3], Stéphanie Descroix[4], Danijela Matic Vignjevic[1], Youmna Attieh[1,5†], Marine Verhulsel[4,5†]

[1]Institut Curie, PSL Research University, CNRS, UMR 144, F-75005 Paris, France
[2]Université Paris Descartes, 12 rue de l'Ecole de Médecine, 75006 Paris
[3]Department of Living Matter, AMOLF, Science Park 104, 1098 XG Amsterdam, The Netherlands
[4] Institut Curie, PSL Research University, CNRS, UMR 168, F-75005 Paris, France
[5]Sorbonne Universités, UPMC Univ Paris06, IFD, 4 Place Jussieu, 75252 PARIS cedex05
[*]Authors contributed equally to this study

[†] Authors contributed equally to this study, corresponding authors :

Youmna Attieh
UMR 144 CNRS/Institut Curie, Institut Curie
25 rue d'Ulm, 75248 Paris cedex 05, France
Tel: +33 (0) 1 42 34 62 01
Fax: +33 (0) 1 42 34 63 77
E-mail : YMAttie@mdanderson.org

Marine Verhulsel
UMR 168 CNRS/Institut Curie, Institut Curie
25 rue d'Ulm, 75248 Paris cedex 05, France
Tel : +33 (0) 1 56 24 64 68
Fax : +33 1 (0) 40 51 06 36
E-mail : marine.verhulsel@gmail.com

This paper is dedicated to the memory of Maxime Dahan, director of the UMR 168, who recently passed away. As a member of the Labex CelTisPhyBio steering committee, he supported this study through grant funding.

Abstract

Tumor initiation and growth is associated with significant changes in the surrounding tissue. During carcinoma progression, a global stiffening of the extracellular matrix is observed and is interpreted as a signature of aggressive invasive tumors. However, it is still unknown if this increase in matrix rigidity promotes invasion and whether this effect is constant along the course of invasion. Here, we have developed a biomimetic *in vitro* assay that enabled us to address the question of the importance of tissue rigidity in the chronology of tumor invasion. Using low concentrations of the sugar threose, we can effectively stiffen reconstituted collagen I matrices and control the stiffening in time with no direct effect on residing cells. Our findings demonstrate that, depending on the timing of its stiffening, the extracellular matrix could either inhibit or promote cancer cell invasion and subsequent metastasis: while matrix stiffening after the onset of invasion promotes cancer cell migration and tumor spreading, stiff matrices encapsulate the tumor at an early stage and prevent cancer cell invasion. Our study suggests that adding a temporal dimension in *in vitro* models to analyze biological processes in 4D is necessary to fully capture their complexity.

Introduction

The tumor microenvironment is characterized by an abnormal synthesis of extracellular matrix (ECM) components and an overall increase of matrix stiffness (Attieh and Vignjevic, 2016; Levental et al., 2009; Paszek et al., 2005). Such severe changes in the microenvironment are integrated at the cellular level. As a result, the transition from a benign to a malignant tumor is not induced by tumor internal signaling alone, but results from a dynamic cross-talk between the tumor and its microenvironment (Attieh and Vignjevic, 2016).

In vivo, massive deposition of collagen and enzymatic collagen crosslinking by lysyl oxidase (LOX) are responsible for tumor matrix stiffening (Barker et al., 2012; Levental et al., 2009). However, their impact on tumor progression is not restricted to a mechanical effect. The increase in collagen density also correlates with a higher number of binding sites available and therefore modifies tumor cell adhesion and migration, while LOX also acts as an intracellular factor regulating genes responsible for epithelial-mesenchymal transition (Attieh and Vignjevic, 2016; Barker et al., 2012; Levental et al., 2009).

Although stiff matrices are a signature of aggressive tumors, the causal connection between matrix stiffness and tumor aggressiveness has never been tested. Does matrix stiffening induce cancer cell invasion or is it a consequence of tumor spreading? And is the effect of matrix stiffness on cancer cell invasion constant in time or do cells respond differently to mechanical changes in their environment depending on whether these happen during early or advanced stages of invasion?

To address these questions, *in vitro* models are valuable tools as they are less complex than the *in vivo* microenvironment and offer the ability to decouple the different parameters at play in cancer invasion. Here, we show a new approach by which we can modify matrix stiffness alone at different time points during tumor invasion. We use threose, a sugar and natural collagen crosslinker (Kinnunen et al., 2012) that is more effective than the traditional crosslinking agent ribose. As threose does not affect cell autonomous adhesion, migration and force generation, we can modulate the stiffness of collagen gels without affecting cancer cells embedded in the gel. Our results expose the importance of the temporal dimensions of biological processes and reveal that matrix stiffening inhibits invasion at an early stage but enhances it at later stage.

Results and discussion

Threose stiffens collagen more efficiently than ribose

In vitro models of tumor-matrix interactions ideally need to recapitulate the fibrillar structure, rheological properties, and the nature and spatial distribution of ligands of the *in vivo* ECM in order to provide biologically relevant insights (Verhulsel et al., 2014). We therefore chose collagen I for our artificial matrix as it supports the growth of cells in 3D while closely mimicking *in vivo* fibrillar ECMs and reproducing cell-matrix interactions specific to tumors (Geraldo et al., 2012; Wolf et al., 2009; Wolf et al., 2013). Amongst the different options published in the literature to stiffen collagen (Levental et al., 2009; Paszek et al., 2005; Tanaka et al., 1988), glycation and LOX crosslinking are the only ones also occurring spontaneously *in vivo*. As LOX activity is known to modulate gene expression, glycation occurring between glucose and collagen better meets our needs for a physiological environment (Tanaka et al., 1988). Ribose is mostly used as a glucose substitute *in vitro* but the high concentrations and long incubation time required to significantly stiffen the collagen matrix are presumed to induce a diabetic phenotype in cells (Han et al., 2011).

To overcome this limitation, we tested an alternative collagen crosslinker, threose, which efficiently forms crosslinks in bovine articular cartilage (Kinnunen et al., 2012). We incubated collagen gels with threose after polymerization to avoid any interference with fibrillogenesis and minimize potential changes in network architecture. To test if threose is a more effective crosslinker than ribose, we compared the rheological properties of 2mg/mL collagen gels alone or supplemented for 48 hours either with 1mM of threose or with 1mM or 10mM of ribose. At concentrations of 1mM, the elastic modulus of collagen treated with ribose was similar to control whereas threose treatment induced a 1.8 fold increase in stiffness (Fig 1A). At a concentration of 10mM, ribose stiffened collagen to the same extent as 1mM threose (Fig 1A).

These results suggest that threose is effective at lower concentrations than ribose, which is advantageous as lower sugar concentrations diminish the likelihood to induce a diabetic phenotype or cause a hypertonic stress to cells.

In addition, monitoring the development of the elastic modulus of collagen gels in time revealed that ribose treatment had a delayed impact on collagen crosslinking compared to threose (Fig. 1B). Measurements of the mesh size of the networks by reflectance microscopy validated that the architecture of collagen networks was not affected by threose (Fig. 1C). This was confirmed by fluorescence microscopy imaging, although this yielded overall

smaller mesh sizes than reflectance imaging because fluorescence microscopy, unlike reflectance imaging, visualizes also fibers orthogonal to the plane of imaging (Fig. 1C). Whether in control or threose-treated gels, mesh sizes similarly varied between 2 and 5µm, indicating that threose did not induce heterogeneous changes in ECM architecture (Fig.1D). Furthermore, we confirmed that the addition of threose did not affect fiber structure by using turbidimetry to compare fiber radii in the absence and presence of threose, which were respectively, 90±7 nm and 88±7 nm. Altogether, this characterization shows that a low concentration of threose is effective in changing the stiffness of collagen gels without altering network architecture.

Collagen stiffening before the onset of invasion inhibits cancer cell invasion

We first considered the influence of matrix stiffening at an early stage, when cancer cell invasion has not yet started. To model tumor invasion *in vitro*, we mixed spheroids of CT26 intestinal adenocarcinoma invasive cells with 2mg/mL collagen solutions. Once collagen polymerized, gels containing spheroids were incubated in 1mM of threose for a 24h or 48h treatment (Fig 2A – Thr_24h; Thr_48h). Invasion was quantified 3 days after embedding. The number of cells that invaded out of the spheroid was counted using a 3D automated software. This quantification method generates an invasion index which represents the number of invading cancer cells normalized to the surface area of the spheroid contour. Therefore, we only scored active cell migration and did not discriminate spheroids based on their size (Attieh et al., 2017).

Matrix stiffening before the onset of invasion dramatically inhibited cell invasion when collagen was treated with threose compared to control (Fig. 2B, C). Treating collagen with threose for an additional day did not further impede the invasion capacity of cancer cells, as it was already almost completely blocked upon a 24h treatment (Fig. 2B, C). Consistent with these findings, CT26 cancer cells invaded collagen gels with slower speed in the presence of threose when embedded as single cells (Fig. 2D). Cell persistence was similar in both conditions, indicating that it was the cells' capacity to move rather than the directional persistence of their movement that was compromised in a stiffer matrix (Fig. 2D).

Inhibition of invasion could be due to an increase in matrix stiffness or to a direct effect of threose on cells. To check whether threose impeded the invasive phenotype of cells, CT26 were pre-incubated in 1mM threose for 3 days while spheroids were forming (Fig. 2A – Thr_incubation). Invasion was similar for pre-incubated and control spheroids, indicating that threose did not alter the invasive phenotype of cancer cells (Fig 2B, C).

We further verified whether threose could alter the molecular machinery driving cell migration by plating cancer cells on glass as an inert substrate that cannot be glycated, and treated with increasing concentrations of threose (Fig. 2E). Cells migrated with equivalent speed and persistence regardless of threose concentration, suggesting that threose did not affect the migratory phenotype of cancer cells.

Alternatively, threose could decrease adhesion of cells to collagen. We tested the latter hypothesis by plating cells on 2D collagen matrices for increment time-points and measuring the percentage of adhered cells after wash (Fig. 2F). We found that cell adhesion was unaffected whether collagen (Coll_thr), cells (Cells_Thr) or both (Cells_Thr + Coll_Thr) were treated with threose compared to control, suggesting that threose did neither modify collagen adhesion sites nor the adhesion capacity of cancer cells (Fig 2F). We thus concluded that the inhibition of invasion at an early stage was only due to matrix stiffening.

Collagen stiffening before the onset of invasion prevents fiber alignment by cancer cells

Previous reports have shown that prior to invasion, cancer cells contract and align collagen fibers in the direction of their movement (Kopanska et al., 2016; Provenzano et al., 2009; Riching et al., 2014). Once collagen is aligned, cancer cells migrate in a fast and persistent manner promoting tumor spreading (Riching et al., 2014). In *in vitro* models, collagen fibers are initially aligned parallel to the edge of the tumor (Kopanska et al., 2016). To evaluate if cells remodeled the matrix, we imaged collagen I fibers surrounding spheroids 3 days post-polymerization and quantified fiber orientation of control and threose-treated gels. Imaging of collagen I revealed that non-crosslinked collagen fibers were not parallel to the edge of the tumor and were randomly organized, while fiber alignment parallel to the spheroid was maintained in threose threated samples (Fig. 3A). This observation was validated by the quantification of the orientation of collagen fibers with respect to the spheroid edge (Fig. 3B). In threose treated collagen gels, fibers were mainly parallel to the spheroid, whereas this tendency was less pronounced in control matrices as the proportion of fibers oriented between 0 and 30° was 20% lower (Fig 3B). We thus concluded that 3 days after spheroid embedding, cells started remodeling collagen fibers in control gels but not in threose-treated samples.

Impaired matrix remodeling observed in threose-treated hydrogels could be either due to a stiffer matrix or to a direct effect of threose on cell mechanisms regulating contractile forces. To test the latter hypothesis, we performed traction force microscopy on cells plated on polyacrylamide gels containing fluorescent beads. Both control and threose-treated cells

exerted comparable traction forces, indicating that threose does not affect traction force generation and that matrix stiffening alone prevented matrix remodeling (Fig. 3C).
Altogether these results suggest that matrix remodeling is necessary for cancer cells to migrate out of the spheroid and that a stiffer matrix inhibits this process.

Collagen stiffening after the onset of invasion favors cancer cell invasion

The reduced invasion we observed in a stiffer environment is surprising, as aggressive tumors are typically characterized by high tissue rigidity. However, it is still not known whether the matrix gets stiffer before or after cancer cell invasion (Attieh and Vignjevic, 2016). Matrix stiffening after the onset of invasion might favor cell invasion, as the critical step of matrix remodeling and fiber alignment is then already complete. To test this hypothesis, we embedded spheroids in collagen and monitored how the invasion rate would change when threose was added after invasion started (i.e. from day 3 to day 5 after embedding spheroids in collagen) (Fig. 4A – Thr_d3d5). Stiffening after the onset of invasion was compared to early stiffening (Thr_d0d2) and control. Experiments were extended to 7 days after embedding spheroids in collagen in order to allow for cells to properly invade out of the spheroid. Similarly to the shorter-term experiments, pre-incubating cancer cells in threose (Fig. 4A - Thr_incubation) did not affect their invasion index compared to control, confirming that threose at a concentration of 1mM does not alter cancer cells' invasive phenotype even at longer times (Fig. 4B, C).
Surprisingly, cancer cell invasion was increased 2-fold when the matrix was stiffened after the onset of invasion compared to control (Fig.4B, C – Thr_d3d5). Moreover, we observed that the decrease of cell invasion observed at day 3 upon threose treatment, before the onset of invasion (Fig. 2B, C), vanished when cancer cells were examined at day 7 (Fig.4B, C – Thr_d0d2): cells showed the same final invasion state as cells invading control gels after 7 days of culture in collagen droplets. This observation indicates that, although matrix stiffening slows down the initiation stage, it enhances cell migration once cells invade the matrix. Given that threose does not interfere with the autonomous migratory phenotype of cancer cells (Fig. 2E), we concluded that matrix stiffening enhances cell migration, resulting in extensive invasion at later stages of tumor development.
Altogether, these experiments highlight the importance of the chronology of events in cancer cell invasion. Depending on the stage of the tumor, the changes in the mechanical properties of its microenvironment could differentially influence its aggressiveness. Matrix stiffening before invasion is initiated slows down the transition from non-invasive to invasive tumor

stage. On the contrary, stiffening of the matrix after the onset of tumor invasion intensifies tumor invasion. We propose here a model whereas, within the chronology of cancer development, cancer cells migrate out of the tumor site, followed by a stiffening of the matrix (Fig. 4D).

We have thus uncovered a novel phenotype of invading tumor cells by effectively modulating matrix stiffness in time without altering cancer cells' autonomous phenotype. We have developed a physiological tumor model composed of spheroids embedded in 3D collagen matrices and selected a natural crosslinker to stiffen collagen. This *in vitro* model allowed us to directly test the correlation between matrix stiffness and tumor aggressiveness observed in patients (Acerbi et al., 2015; Cox and Erler, 2011; Pickup et al., 2014).

As opposed to other crosslinkers commonly used in the field, threose presents the advantage of effectively stiffening collagen at low concentrations. As proven by our experiments, a strong advantage of using threose is that it does not induce changes in the network architecture in terms of mesh size and fibril diameter, while being effective in changing the stiffness of the matrix. This increase in stiffness is most likely due to a stabilization and an increase in crosslinking of already existing contact points.

Using threose at low concentrations allowed us to modify matrix stiffness while tumor cells were embedded in their physiological 3D matrix, as opposed to studies exposing cancer cells to previously treated and already stiff gels, or collagen gels of varying densities that cannot be modulated in time (Krndija et al., 2010; Levental et al., 2009; Paszek et al., 2005; Provenzano et al., 2009). We were thus able to control the temporal onset of matrix stiffening. Although we worked at lower collagen concentration and thereby at lower stiffness than analogous studies using ribose, cells were highly responsive suggesting that cells are more sensitive to relative changes in matrix rigidity than to its intrinsic value (Bordeleau et al., 2017; Carey et al., 2017).

At an early stage of invasion, cells first remodel the matrix to effectively migrate out of the tumor niche. Contractile forces of cancer cells are required to deform the ECM and lead to tensile radial forces within the matrix that orient the collagen fibers perpendicular to the surface of the tumor (Kopanska et al., 2016; Provenzano et al., 2009; Riching et al., 2014). As there is a mechanical relation between the tensile state of the ECM and invasion, collagen organization at the onset of invasion plays a critical role towards the outcome of tumor development. Our results support this hypothesis as threose-treated matrices are stiffer and therefore more difficult to remodel than control matrices. This is evidenced by the high

proportion of collagen fibers oriented parallel to the edge of the tumor 3 days after embedding and the consequent inhibition of cancer cell invasion.

Stiffer matrices are also known to favor a migratory phenotype in cancer cells (Levental et al., 2009; Paszek et al., 2005). This biomechanical process is consistent with the cell response observed when we added threose after the onset of invasion, which led to a two-fold increase in invasion. This antagonistic influence of matrix stiffening in the early and late stages of invasion is clearly illustrated by the behavior of cancer cells when collagen is exposed to threose in the early stage: although the transition from non-invasive to invasive phenotype is delayed compared to control, once invasion is initiated, migration is enhanced as cancer cells catch up with control conditions within 4 days of invasion. As CT26 are invasive cancer cells with a mesenchymal-like phenotype, this result is consistent with new findings suggesting that only malignant cancer cells have the ability to adjust to collagen matrices of different densities (Wullkopf et al., 2018).

In conclusion, our *in vitro* 3D culture model provides a physiologically relevant microenvironment to study the effect of matrix stiffness per se on the transition from benign to malignant tumor. We report here the first data on *in vitro* collagen crosslinking using threose, which allows to significantly stiffen collagen matrices without interfering with the phenotype of cancer cells. Furthermore, this study highlights the need to introduce a fourth dimension into cell biological models. Indeed, a static assay where all factors are initially set and remain unchanged could fail to capture the complexity of cancer invasion. The flexibility of our system allowed us to tackle the question of the dynamics of matrix stiffening during tumorigenesis. Our study illustrates that within the chronology of tumor development, neither matrix stiffening nor softening are the most favorable, but rather an interchanging state that is used by cancer cells to efficiently invade.

Material and Methods

Rheological measurements

Rheology tests were performed on an Anton Paar Physica MCR 501 rheometer, with a stainless steel 30 mm diameter and 1° truncation angle cone-plate geometry (CP30-1). The plates were heated to 37° before loading the sample. Water was added to the solvent trap to maintain a moist environment. 20 minutes after loading the sample, a solution of either pure DMEM, or DMEM supplemented with 1-10mM ribose or 1mM threose was placed around the geometry and allowed to diffuse in the sample for 48 hours. To prevent evaporation during the measurement, a layer of mineral oil was further added around the measuring geometry. During the whole 48h, the elastic and viscous moduli of the network were probed by applying an oscillatory deformation with 0.5% strain amplitude and a frequency of 0.5 Hz. Results show the values of elastic and viscous moduli after 48 hours, averaged over at least three different independent repeats, while the error reported is the standard error of the mean.

Sample preparation

The samples were prepared on ice to prevent early polymerization of collagen. First, collagen was pipetted into an Eppendorf tube and weighed to determine the volume of the final solution. Samples were prepared to have a final collagen concentration of 2 mg/ml, in phosphate buffer saline (PBS) and pH set to 7 with addition of NaOH and topped up to the final volume with DMEM.

Imaging 3D collagen networks

The pure and threose supplemented collagen networks were imaged in confocal reflectance and confocal fluorescence mode using an inverted Eclipse Ti microscope (Nikon, Tokyo, Japan), a 488 nm Argon laser (Melles Griot, Albuquerque, NM) for illumination and a 100× objective (Nikon, N.A. 1.49). Z-stacks were acquired 10 μm above the coverslip to avoid surface effects, over a depth of 10 μm, with a step of 0.2 μm and shown as a maximum projection. The networks were allowed to polymerize for 48 hours at 37°C with controlled humidity. To visualize fluorescent collagen, we added the collagen binding protein CNA35 (Aper et al., 2014) tagged with eGFP (pET28a-EGFP-CNA35 was a gift from Maarten Merkx (Addgene plasmid # 61603)) to collagen prior to polymerization in a molar ratio of 20:1.

Mesh size analysis

The mesh size of the networks was determined using an algorithm described in (Kaufman et al., 2005). Images were background-subtracted and binarized with an Otsu threshold using ImageJ. The resulting image was then analyzed in a custom-written Python routine, which counted the distance between on and off pixels along the rows and columns. The distances obtained were then fitted with an exponential probability distribution and the mean value (converted from pixels to μm) was taken as the average mesh size. For each condition, we analyzed at least 8 randomly sampled images.

Fiber diameter analysis

To analyze the average diameters of the collagen fibers, we performed turbidity measurements with a Lambda 35 dual-beam spectrophotometer (PerkinElmer, Waltham, MA). Samples were polymerized inside a plastic cuvette (UV-Cuvette micro, Plastibrand, Germany) or a quartz cuvette for 48h before measuring. Subsequently, the optical density of the sample was measured in the wavelength range 650-900 nm. The measured optical density I_0 was converted into turbidity τ using the formula:

$$\tau = \frac{I_0 \ln(10)}{L}$$

where L represents the optical path length. To extract fiber radii and mass-length ratios, we employed the following relation (Yeromonahos et al., 2010):

$$\tau\lambda^5 = A\mu(\lambda^2 - Ba^2)$$

Where A and B are constants corresponding respectively to $(88/15)c_p\pi^3 n_s(dn/dc_p)^2/N_A$ and $(184/154)\pi^2 n^2_s$. Here, c_p represent the collagen concentration, n_s the refractive index of the solvent, dn/dc_p is the refractive index increment, N_A is the Avogadro constant, μ the mass per length ratio and *a* the fiber radius.

Cell lines

Mouse intestinal cancer cells CT26 were obtained from American Type Culture Collection (ATCC). Cells were cultured in Dulbecco's Modified Eagle Medium (DMEM) (Life Technologies) supplemented with 10% FBS (Invitrogen) and 5% CO_2. Mycoplasma testing was performed every 2 weeks in order to verify that cells were clear of infections.

Invasion assay

Agarose (Invitrogen) was dissolved in water to a concentration of 0.01g/mL and boiled. 150µL of the solution were added to wells of a 48 well-plate and agarose was left to polymerize for at least 10min at RT. A solution of 10^4 cells/mL of CT26 cancer cells was made, and 75 to 100 µL of the solution was added to the wells. The wells were subsequently filled with DMEM supplemented with 10% FBS +/- threose (1mM, T7642, Sigma) and spheroids were left to form for 3 to 4 days.

$30mm^2$ tissue culture plates were specifically fashioned for the invasion assay: 3 holes of approximately 3-4mm in diameter were drilled in a plate and widened around the edges using a scalpel.

2mg/mL rat tail collagen I (Corning) was prepared in DMEM, 10X PBS and 1M NaOH, to a pH=7 as described in **sample preparation**. The solution was kept on ice in order to avoid collagen polymerization. Spheroids were embedded in 15µL collagen drops, positioned in the hole of the culture plate. After filling all 3 holes, the plate was flipped every 30s for 5min, in

order for the cells to stay in the middle of the collagen drop (preventing sedimentation of spheroids to the glass or to collagen/air interface). Collagen was left to polymerize for an additional 15min at room temperature before 3mL of DMEM supplemented with 5% FBS, 1% AA were added, +/- 1mM of threose.

3D Immunofluorescence

Spheroids embedded in collagen were fixed using 4% paraformaldehyde (PFA) in PBS for 30min at RT. Spheroids were then washed with PBS and permeabilized with 0.1% Triton X-100 in PBS for 30min at RT. DNA and F-actin were stained using DAPI and Phalloidin respectively (Life Technologies). Collagen was imaged using confocal reflection microscopy.

Imaging 3D spheroids

Images were acquired with an inverted AOBS two-photon laser scanning confocal microscope SP8 (Leica) coupled to femtosecond laser Chameleon Vision II (Coherent Inc) using 25x/1.0NA water-immersion objective. The microscope is equipped with two non-descanned HyD detectors: NDD1 (500–550 nm) andNDD2 (≥590nm). Fluorescence channels were recorded simultaneously using the excitation wavelength 980nm. Collagen was visualized by confocal reflectance microscopy, using light at a wavelength of 488 nm and a standard photomultiplier tube (PMT) detector, at a low gain (500V). 3D stacks were obtained at a step size of 2 µm intervals. The images were processed with Leica Application Suite (LAS), ImageJ (NIH) and Imaris (Bitplane).

Invasion counter software

Quantification of cell invasion from spheroids was performed as already described using a custom semi-automated image analysis program written in Python (Attieh et al., 2017).

Cell adhesion assay

CT26 cells were pre-treated for two days with 1mM of threose or no threose in DMEM supplemented with 10% FBS and 1% AA. 50µL of collagen (2m/mL) was polymerized in 96-well plates and was pre-treated for two days with 1mM of threose or no threose in DMEM and 1% AA. After two days, CT26 cells were stained with CellTracker™ Red CMTPX Dye (ThermoFisher) and 2.10^5 cells were seeded per well in the 96-well plate. Cells were then incubated at 37ºC for 5min, 15min, 30min, 1h or 2h and washed three times to remove non-adherent cells. Fluorescence intensity was measured using a FluoStar fluorescence plate reader (BMG Labtech). Adhesion was represented as the percentage of adherent cells per condition.

Collagen topography measurements

Fibers alignment and their angles with respect to the spheroid edge were measured on images acquired using reflection microscopy with the available software CurveAlign (UW-Madison; http://loci.wisc.edu/software/curvealign) in MatLab. The angles of collagen fibers compared to the spheroid edge were determined for 7-8 slices per condition.

Traction force microscopy

Traction force microscopy was conducted as previously described (Elkhatib et al., 2014).
35mm glass-bottom cell culture dishes (FluoroDish, World Precision Instruments) were silanized with (3-aminopropyl)trimethoxysilane (Sigma-Aldrich) for 15min and extensively washed with water. The glass surface of the dishes was treated with 0.5% glutaraldehyde (Electron Microscopy sciences) for 30min and extensively washed with water. Acrylamide 40% (93.3µL) and 2% bisacrylamide (11µL) were mixed in PBS solution to a final volume of 500µL to achieve a Young's modulus of 5 kPa. For traction force measurements, FluoSphere bead solution (0.2 µm, 580/605 nm; Invitrogen) was added at 2% volume. Polymerization was initiated by addition of 2.5µL ammonium persulfate (10% w/v solution) and 0,25µL of N,N,N',N'-tetramethylethane-1,2-diamine (TEMED). 12µL of the polyacrylamide solution was rapidly deposited onto the glass-bottom dish and covered with a 18mm coverslip. After one hour PBS was added to the dishes for 10min and the coverslips were gently removed under PBS. To allow for collagen coating, the gel surface was activated using Sulfo-SANPAH (1mg/mL, ThermoFisher) that was photoactivated by UV (365nm) for 10min. After 3 washes with HEPES and PBS, the gels were coated with monomeric collagen (100µg/mL) overnight at 4°C. The next day gels were washed 3 times with PBS. CT26 cells were pre-treated for 1 day with +/- 1mM threose prior to seeding on the gels. 1.10^4 CT26 cells were plated per gel in DMEM supplemented with 10% FBS, 2% AA, +/- 1mM threose and cultured on the gels one additional day, thus allowing for a total two-day incubation with +/- threose.
To image traction force experiments, we used an Inverted Nikon Ti-E microscope equipped with a sCMOS 2048 ORCA Flash4.0 V2 camera (Hamamatsu) and a 40x Plan Fluor dry objective (0.75 NA; Nikon). A fluorescent image of the FluoSphere beads and a phase contrast image of the cells were acquired. At the end of the acquisition cells were detached from the gels using 0.5% Trypsin-EDTA (Gibco) and a reference image without cells was recorded. We used a previously described correlation algorithm to extract the bead displacement fields. Traction force was determined using the Fourier transform traction force algorithm, as introduced by (Butler et al., 2002). To quantify the force applied by a cell, we measured the strain energy that corresponds to the energy the cell exerts to deform the substrate, which is proportional to the average force applied by a cell.

2D migration

CT26 cells were incubated for two days with the following concentrations of threose: 0mM, 0.5mM, 1mM and 2mM in DMEM supplemented with 10% FBS and 1% AA. After two days, CT26 were resuspended and 2500 cells were seeded on uncoated glass-bottom wells of a 96-well plate. After overnight imaging, all the wells were washed and DMEM 10% FBS 1% AA was added, and cell migration was imaged for 8 more hours. .

3D migration of single cells

2mg/mL rat tail collagen I (Corning) was prepared in DMEM, 10X PBS and 1M NaOH, to a pH=7 as described in sample preparation. The solution was kept on ice in order to avoid collagen polymerization. Glass-bottom cell culture dishes (FluoroDish, World Precision Instruments) were coated with poly-L-Lysine (Sigma-Aldrich) for 5min, and washed 3 times

with PBS. CT26 cells were resuspended and 5000 cells were embedded in 40µL collagen drops that were deposited on the bottom of the culture dishes. Dishes were flipped for 1.5min, in order for the cells to stay in the center of the collagen drop. Collagen was left to polymerize for an additional 30min at room temperature before 2mL of DMEM supplemented with 10% FBS, 1% AA were added, +/- 1mM of threose. Dishes were maintained for two days at 37°C, 5% CO2.

Microscopy of CT26 migration and image analysis

2D and 3D culture were imaged using an Inverted Nikon Ti-E microscope equipped with a sCMOS 2048 ORCA Flash4.0 V2 camera (Hamamatsu) using the following objectives: Plan Fluor 10x Ph1 DL and Plan Apo VC 20x DIC N2. Images were acquired every 10 to 20min for 8 to 12h.

A random population of cells was selected and manually tracked in 2D using the MTrackJ plugin (Meijering et al., 2012) in ImageJ (Bitplane). Following tracking of cells, the trajectories were analyzed using custom software written in Python. Migration persistence was defined as the final cell displacement divided by the length of the trajectory.

Statistical analysis

All experiments were performed in a minimum of 3 independent experiments. All statistical analysis and graphic representations were performed using Prism software.

Acknowledgements

We thank Andrew G. Clark for designing the 3D quantification software, Carlos Perez-Gonzalez for help with the generation of roseplots, Marko Matic for help with quantification of 2D migration data, Nadia Elkhatib and Jorge Barbazan for help with TFM and cell adhesion. We acknowledge Nikon Imaging Center@CNRS-Institut Curie, PICT-IBiSA@Lhomond supported by the Fondation pour la Recherche Médicale (FRM N° DGE20111123020), the Cancérôple-IdF (n°2012-2-EML-04-IC-1), InCA (Cancer National Institute, n° 2011-1-LABEL-IC-4). We also thank La ligue contre le cancer (Y.A. and M.V.), and Fondation pour la Recherche Médicale (FRM FDT20170437130) and Ecole Doctorale Frontières du Vivant (FdV) – Programme Bettencourt (RS). The work of F.B. and G.H.K. is part of the Industrial Partnership Programme Hybrid Soft Materials that is carried out under an agreement between Unilever Research and Development B.V. and the Netherlands Organisation for Scientific Research (NWO). This work was supported by Labex CelTisBioPhy (Y.A and M.V.).

The authors declare no competing financial interests.

Y.A and M.V conceived the study under the supervision of D.M.V and S.D. R.S and Y.A performed the cell biology experiments. F.B performed all experiments on collagen rheology and collagen network mesh size and diameter, under the supervision of G.H.K. Y.A and M.V wrote the manuscript with input from all authors.

References

Acerbi, I., L. Cassereau, I. Dean, Q. Shi, A. Au, C. Park, Y.Y. Chen, J. Liphardt, E.S. Hwang, and V.M. Weaver. 2015. Human breast cancer invasion and aggression correlates with ECM stiffening and immune cell infiltration. *Integr Biol (Camb)*. 7:1120-1134.

Aper, S.J., A.C. van Spreeuwel, M.C. van Turnhout, A.J. van der Linden, P.A. Pieters, N.L. van der Zon, S.L. de la Rambelje, C.V. Bouten, and M. Merkx. 2014. Colorful protein-based fluorescent probes for collagen imaging. *PLoS One*. 9:e114983.

Attieh, Y., A.G. Clark, C. Grass, S. Richon, M. Pocard, P. Mariani, N. Elkhatib, T. Betz, B. Gurchenkov, and D.M. Vignjevic. 2017. Cancer-associated fibroblasts lead tumor invasion through integrin-beta3-dependent fibronectin assembly. *J Cell Biol*.

Attieh, Y., and D.M. Vignjevic. 2016. The hallmarks of CAFs in cancer invasion. *Eur J Cell Biol*. 95:493-502.

Barker, H.E., T.R. Cox, and J.T. Erler. 2012. The rationale for targeting the LOX family in cancer. *Nat Rev Cancer*. 12:540-552.

Bordeleau, F., B.N. Mason, E.M. Lollis, M. Mazzola, M.R. Zanotelli, S. Somasegar, J.P. Califano, C. Montague, D.J. LaValley, J. Huynh, N. Mencia-Trinchant, Y.L. Negron Abril, D.C. Hassane, L.J. Bonassar, J.T. Butcher, R.S. Weiss, and C.A. Reinhart-King. 2017. Matrix stiffening promotes a tumor vasculature phenotype. *Proc Natl Acad Sci U S A*. 114:492-497.

Butler, J.P., I.M. Tolic-Norrelykke, B. Fabry, and J.J. Fredberg. 2002. Traction fields, moments, and strain energy that cells exert on their surroundings. *Am J Physiol Cell Physiol*. 282:C595-605.

Carey, S.P., K.E. Martin, and C.A. Reinhart-King. 2017. Three-dimensional collagen matrix induces a mechanosensitive invasive epithelial phenotype. *Sci Rep*. 7:42088.

Cox, T.R., and J.T. Erler. 2011. Remodeling and homeostasis of the extracellular matrix: implications for fibrotic diseases and cancer. *Dis Model Mech*. 4:165-178.

Elkhatib, N., M.B. Neu, C. Zensen, K.M. Schmoller, D. Louvard, A.R. Bausch, T. Betz, and D.M. Vignjevic. 2014. Fascin plays a role in stress fiber organization and focal adhesion disassembly. *Curr Biol*. 24:1492-1499.

Geraldo, S., A. Simon, N. Elkhatib, D. Louvard, L. Fetler, and D.M. Vignjevic. 2012. Do cancer cells have distinct adhesions in 3D collagen matrices and in vivo? *Eur J Cell Biol*. 91:930-937.

Han, C., Y. Lu, Y. Wei, Y. Liu, and R. He. 2011. D-ribose induces cellular protein glycation and impairs mouse spatial cognition. *PLoS One*. 6:e24623.

Kaufman, L.J., C.P. Brangwynne, K.E. Kasza, E. Filippidi, V.D. Gordon, T.S. Deisboeck, and D.A. Weitz. 2005. Glioma expansion in collagen I matrices: analyzing collagen concentration-dependent growth and motility patterns. *Biophys J*. 89:635-650.

Kinnunen, J., H.T. Kokkonen, V. Kovanen, M. Hauta-Kasari, P. Vahimaa, M.J. Lammi, J. Toyras, and J.S. Jurvelin. 2012. Nondestructive fluorescence-based quantification of threose-induced collagen cross-linking in bovine articular cartilage. *J Biomed Opt*. 17:97003.

Kopanska, K.S., Y. Alcheikh, R. Staneva, D. Vignjevic, and T. Betz. 2016. Tensile Forces Originating from Cancer Spheroids Facilitate Tumor Invasion. *PLoS One*. 11:e0156442.

Krndija, D., H. Schmid, J.L. Eismann, U. Lother, G. Adler, F. Oswald, T. Seufferlein, and G. von Wichert. 2010. Substrate stiffness and the receptor-type tyrosine-protein phosphatase alpha regulate spreading of colon cancer cells through cytoskeletal contractility. *Oncogene*. 29:2724-2738.

Levental, K.R., H. Yu, L. Kass, J.N. Lakins, M. Egeblad, J.T. Erler, S.F. Fong, K. Csiszar, A. Giaccia, W. Weninger, M. Yamauchi, D.L. Gasser, and V.M. Weaver. 2009. Matrix crosslinking forces tumor progression by enhancing integrin signaling. *Cell*. 139:891-906.

Meijering, E., O. Dzyubachyk, and I. Smal. 2012. Methods for cell and particle tracking. *Methods Enzymol*. 504:183-200.

Paszek, M.J., N. Zahir, K.R. Johnson, J.N. Lakins, G.I. Rozenberg, A. Gefen, C.A. Reinhart-King, S.S. Margulies, M. Dembo, D. Boettiger, D.A. Hammer, and V.M. Weaver. 2005. Tensional homeostasis and the malignant phenotype. *Cancer Cell*. 8:241-254.

Pickup, M.W., J.K. Mouw, and V.M. Weaver. 2014. The extracellular matrix modulates the hallmarks of cancer. *EMBO Rep*. 15:1243-1253.

Provenzano, P.P., D.R. Inman, K.W. Eliceiri, and P.J. Keely. 2009. Matrix density-induced mechanoregulation of breast cell phenotype, signaling and gene expression through a FAK-ERK linkage. *Oncogene*. 28:4326-4343.

Riching, K.M., B.L. Cox, M.R. Salick, C. Pehlke, A.S. Riching, S.M. Ponik, B.R. Bass, W.C. Crone, Y. Jiang, A.M. Weaver, K.W. Eliceiri, and P.J. Keely. 2014. 3D collagen alignment limits protrusions to enhance breast cancer cell persistence. *Biophys J*. 107:2546-2558.

Tanaka, S., G. Avigad, B. Brodsky, and E.F. Eikenberry. 1988. Glycation induces expansion of the molecular packing of collagen. *J Mol Biol*. 203:495-505.

Verhulsel, M., M. Vignes, S. Descroix, L. Malaquin, D.M. Vignjevic, and J.L. Viovy. 2014. A review of microfabrication and hydrogel engineering for micro-organs on chips. *Biomaterials*. 35:1816-1832.

Wolf, K., S. Alexander, V. Schacht, L.M. Coussens, U.H. von Andrian, J. van Rheenen, E. Deryugina, and P. Friedl. 2009. Collagen-based cell migration models in vitro and in vivo. *Semin Cell Dev Biol*. 20:931-941.

Wolf, K., M. Te Lindert, M. Krause, S. Alexander, J. Te Riet, A.L. Willis, R.M. Hoffman, C.G. Figdor, S.J. Weiss, and P. Friedl. 2013. Physical limits of cell migration: control by ECM space and nuclear deformation and tuning by proteolysis and traction force. *J Cell Biol*. 201:1069-1084.

Wullkopf, L., A.V. West, N. Leijnse, T.R. Cox, C.D. Madsen, L.B. Oddershede, and J.T. Erler. 2018. Cancer cell ability to mechanically adjust to extracellular matrix stiffness correlates with their invasive potential. *Mol Biol Cell*:mbcE18050319.

Yeromonahos, C., B. Polack, and F. Caton. 2010. Nanostructure of the fibrin clot. *Biophys J*. 99:2018-2027.

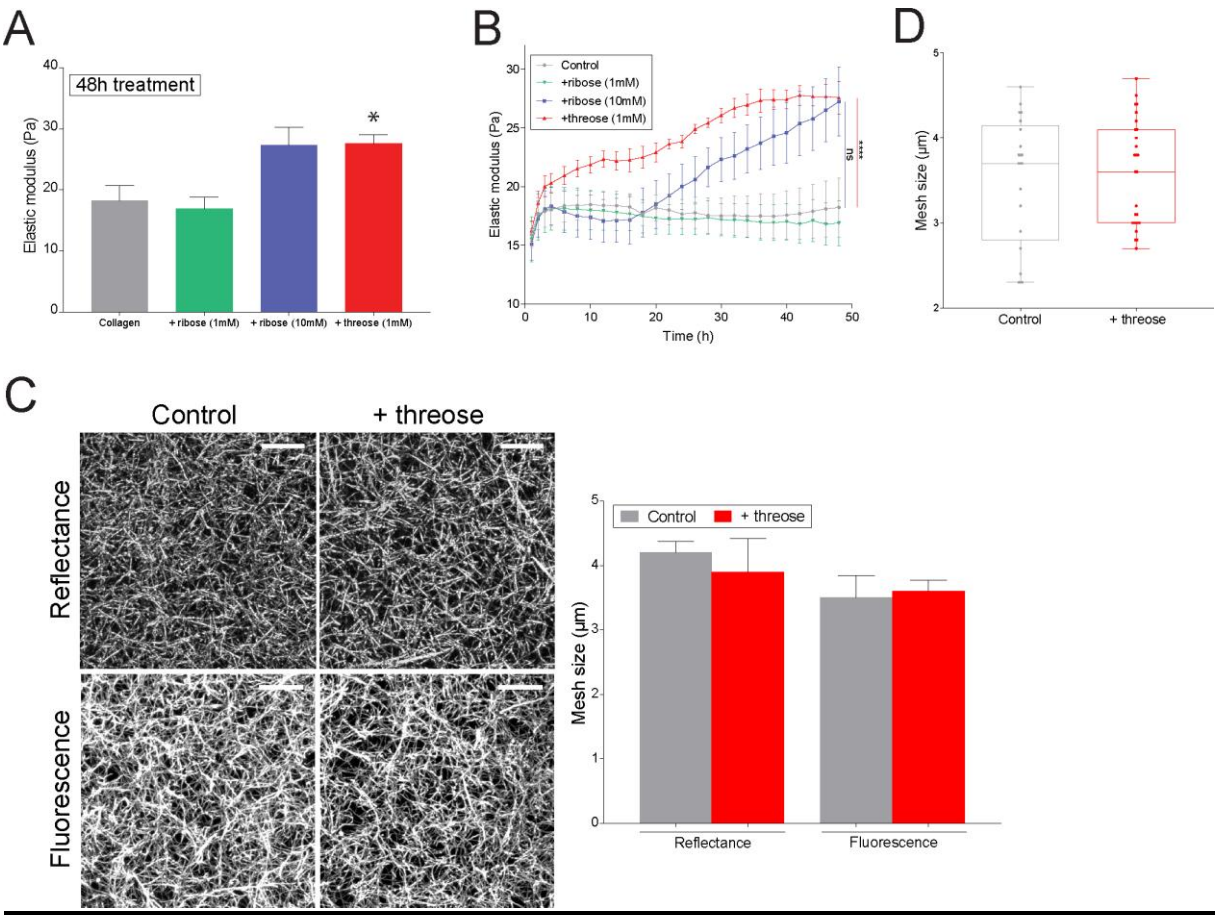

Figure 1: Threose stiffens collagen more efficiently than ribose

(A) Elastic moduli obtained with small amplitude oscillatory rheology for untreated collagen gels, gels treated with 1 mM or 10 mM of ribose or with 1 mM threose, 48 hours after polymerization. Data represents an average over at least three independent measurements. p values are compared to control condition using Dunnett's multiple comparison test (*p<0.05, **p<0.01, ***p<0.001).

(B) Measurements of elastic moduli as a function of time over a period of 48h obtained with small amplitude oscillatory rheology on untreated collagen gels, gels treated with 1mM or 10mM of ribose, or with 1mM threose. Results are expressed as mean +/- SEM obtained as an average over at least three independent measurements. p values are compared to control condition using Dunnett's multiple comparison test (*p<0.05, **p<0.01, ***p<0.001).

(C) **Left:** Maximum intensity projections of reflectance and fluorescence images of collagen networks with or without 1mM of threose added during 48h. Scale bar = 10µm. **Right:** Mesh size measurements of collagen networks. Results are represented as a histogram with mean + SEM for n=8 positions over n=3 independent samples. p values were calculated using an unpaired t-test for each separate condition and showed no statistical difference. The mesh size measured with fluorescence microscopy is smaller because confocal reflectance does not allow for visualization of fibers perpendicular to the imaging plane.

(D) Mesh size distribution within collagen networks acquired by fluorescence. Results are represented as box and whiskers (minimum to maximum), where each point represents a different region within the matrix, with n > 20 positions over n=3 independent samples. p values were calculated using an unpaired t-test for each separate condition and showed no statistical difference.

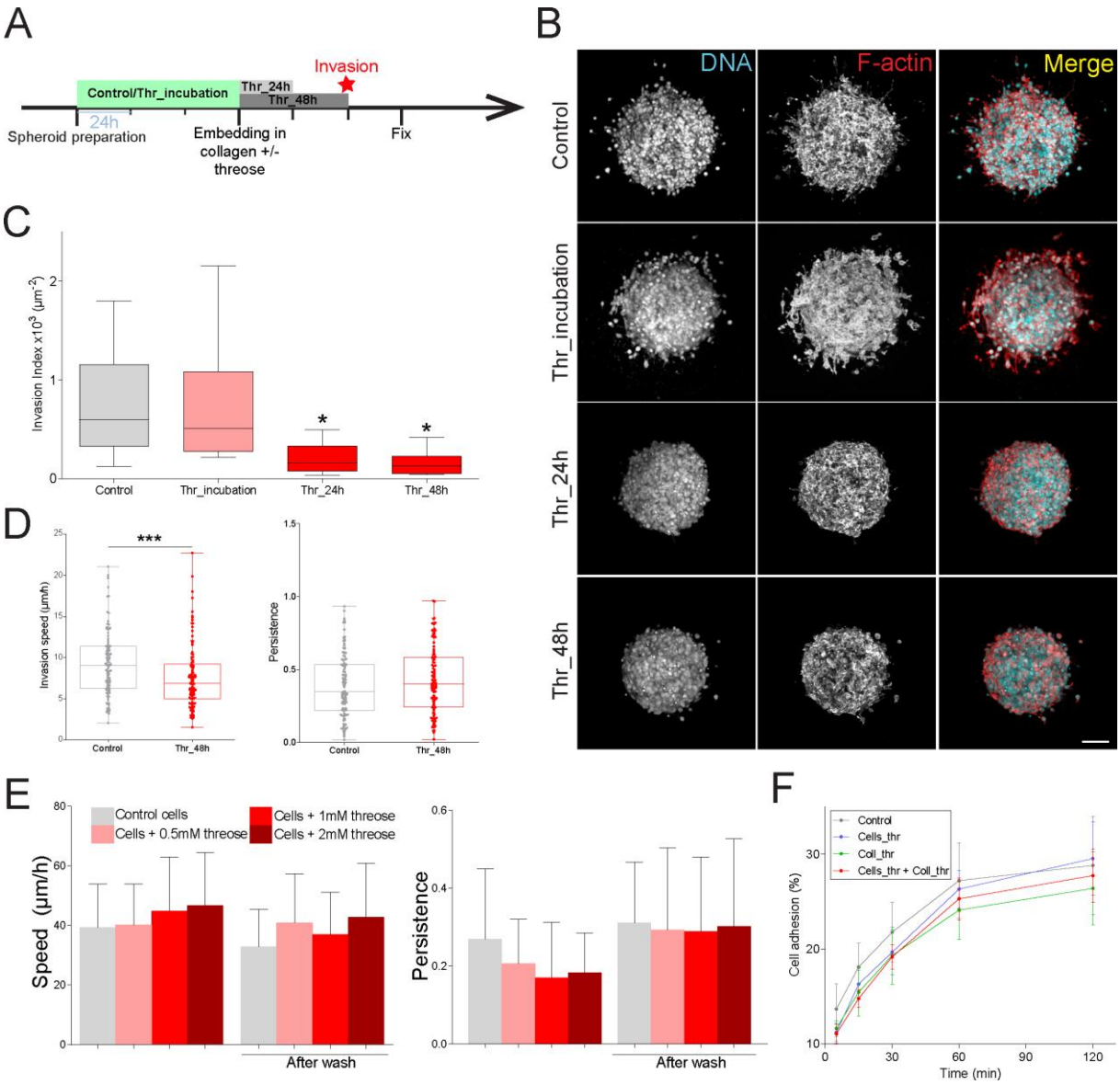

Figure 2: Collagen stiffening before the onset of invasion inhibits cancer cell invasion

(A) Timeline representing the chronology of the experiment. Cancer cell were plated in agarose-coated wells for 3 days to form spheroids, in the absence (Control) or presence of threose (Thr_incubation). Spheroids were then embedded in collagen droplets with or without threose. Threose was washed out 24h (Thr_24h) and 48hours (Thr_48h) later. All spheroids were fixed at day 3 post-embedding.

(B) Maximum intensity projections of cancer cell spheroids at day 3. F-actin (red) and DNA (cyan) were respectively stained with phalloidin-rhodamin and DAPI. Scale bar indicates 100µm.

(C) Quantification of cancer cell invasion. Invasion index is defined as the ratio between the number of invading nuclei of cancer cells and the area of the spheroid contour. Data are expressed as box and whiskers (minimum to maximum) of at least N=3 separate experiments. p values are compared to control condition using Newman-Keuls multiple comparison test (*p<0.05, **p<0.01, ***p<0.001).

(D) Quantification of single cell invasion/migration in 3D collagen gels (left: speed; right: persistence) +/- 1mM of threose, after a 48h incubation in threose. Persistence was defined as the final cell displacement divided by the length of the trajectory. Results are represented as box and whiskers (minimum to maximum) where each point represents an individual cell. P-value was calculated using Mann–Whitney test for n = 107 cells for control and n = 105 cells for threose, over n = 3 separate experiments (*p<0.05, **p<0.01, ***p<0.001).

(E) Quantification of migration (left: speed; right: persistence) of CT26 cancer cells with increasing concentrations of threose treatment plated on glass. Measurements were performed during threose treatment and after wash. Migration persistence was defined as the final cell displacement divided by the length of the

trajectory. Results are represented as a histogram with mean + SD for 3 independent experiments. p values were calculated using Newman-Keuls multiple comparison test and showed no statistical difference.

(F) Quantification of the capacity of control cells to adhere to collagen (control, grey) or to threose-treated collagen (Coll_thr, green), and of threose-treated cells to adhere to control collagen (Cells_thr, blue) or to threose-treated collagen (Cells_thr + coll_thr, red). Measurements were performed at 0, 15min, 30min, 1h and 2h. Results are expressed as an XY coordinate with mean +/- SD with data representing an average over three independent measurements. p values are compared to control condition using Dunnett's multiple comparison test and showed no statistical difference.

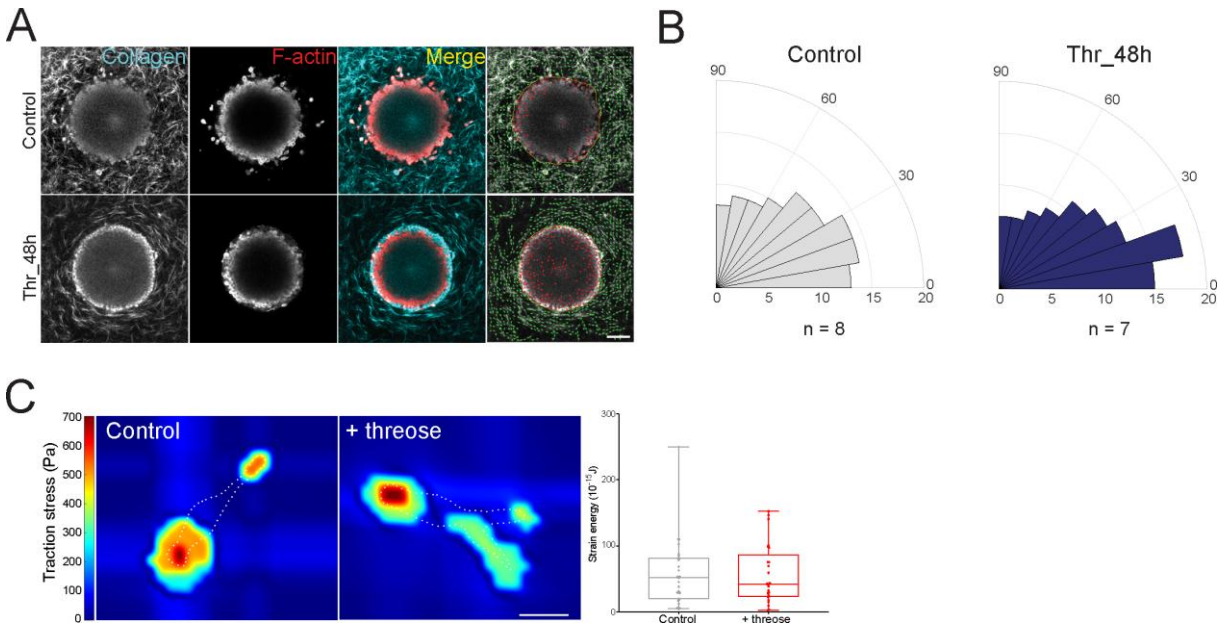

Figure 3: Collagen stiffening before the onset of invasion prevents fiber alignment by cancer cells

(A) 2D slices of cancer cell spheroids in collagen I at day 3. F-actin (red) was stained with phalloidin-rhodamine and collagen was imaged using reflectance (cyan). **Right panel:** overlaid images of collagen I matrices containing cancer cell spheroids generated using the software CurveAlign (UW-Madison; http://loci.wisc.edu/software/curvealign). Yellow line indicates the edge of the spheroid and green lines indicate fibers orientation with respect to the closest point on the spheroid edge. Scale bar = 100µm.

(B) Rose plots representing the frequency of distribution of the absolute angles of collagen fibers within the range of 0 to 90° with respect to the closest point on the spheroid edge. Data represent the average of 7 <n <8 spheroids. Fibers parallel to the tumor edge lie in the 0-30° angles.

(C) **Left:** Representative traction force map of a control and a threose-treated cell on collagen-coated polyacrylamide gels with Young's modulus of 5 kPa. White dotted line represents the cell's edge. Color code gives the magnitude of traction stress in Pa, which corresponds to forces of (pN/µm2). Scale bar = 20µm. **Right:** Corresponding mean force (strain energy) exerted by CT26 cancer cells. Results are represented as box and whiskers (minimum to maximum) where each point represents an individual cell. P-value was calculated using Mann–Whitney test for *n* = 27 cells for control and n = 25 cells for threose over 3 separate experiments and showed no statistical difference.

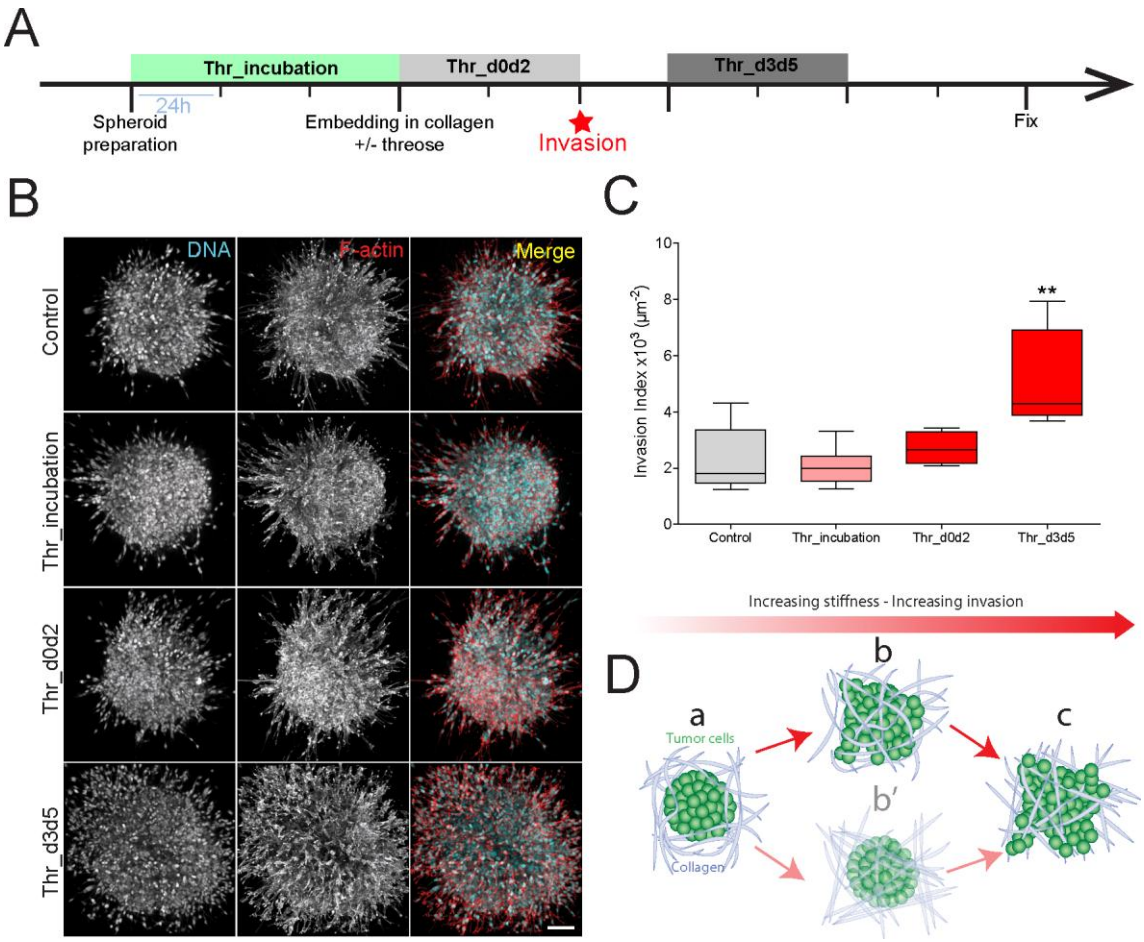

Figure 4: Collagen stiffening after the onset of invasion favors cancer cell invasion

(A) Timeline representing the chronology of the experiment. Cancer cell spheroids were left to form in agarose-coated wells for 3 days, with (Thr_incubation) or without threose (Control). Spheroids were then embedded in collagen droplets with (Thr_d0d2) or without (Control) threose for 48hours. 3 days post-embedding, threose was added in the media for 48h (Thr_d3d5). All spheroids were fixed at day 7 post-embedding.

(B) Maximum intensity projections of cancer cell spheroids at day 7. F-actin (red) and DNA (cyan) were respectively stained with phalloidin-rhodamin and DAPI. Scale bar indicates 100µm.

(C) Quantification of cancer cell invasion. Invasion index is defined as the ratio between the number of invading nuclei of cancer cells and the area of the spheroid contour. Quantification results are expressed as box and whiskers (minimum to maximum) of N=3 separate experiments. p values are compared to control condition using Newman-Keuls multiple comparison test (*p<0.05, **p<0.01, ***p<0.001).

(D) Model: tumor cells are surrounded by the ECM (a). Cancer cells start invading the ECM before the matrix gets remodeled (b) rather than the matrix being remodeled beforehand (b'). As cancer cells invade the matrix, collagen fibers get aligned, which sets up positive feedback to enhance invasion.